JCI The Journal of Clinical Investigation

Targeting SOD1 reduces experimental non–small-cell lung cancer

Andrea Glasauer, … , Andrew P. Mazar, Navdeep S. Chandel

J Clin Invest. 2014;124(1):117-128. https://doi.org/10.1172/JCI71714.

Research Article **Oncology**

Approximately 85% of lung cancers are non–small-cell lung cancers (NSCLCs), which are often diagnosed at an advanced stage and associated with poor prognosis. Currently, there are very few therapies available for NSCLCs due to the recalcitrant nature of this cancer. Mutations that activate the small GTPase KRAS are found in 20% to 30% of NSCLCs. Here, we report that inhibition of superoxide dismutase 1 (SOD1) by the small molecule ATN-224 induced cell death in various NSCLC cells, including those harboring *KRAS* mutations. ATN-224–dependent SOD1 inhibition increased superoxide, which diminished enzyme activity of the antioxidant glutathione peroxidase, leading to an increase in intracellular hydrogen peroxide (H_2O_2) levels. We found that ATN-224–induced cell death was mediated through H_2O_2-dependent activation of P38 MAPK and that P38 activation led to a decrease in the antiapoptotic factor MCL1, which is often upregulated in NSCLC. Treatment with both ATN-224 and ABT-263, an inhibitor of the apoptosis regulators BCL2/BCLXL, augmented cell death. Furthermore, we demonstrate that ATN-224 reduced tumor burden in a mouse model of NSCLC. Our results indicate that antioxidant inhibition by ATN-224 has potential clinical applications as a single agent, or in combination with other drugs, for the treatment of patients with various forms of NSCLC, including *KRAS*-driven cancers.

Targeting SOD1 reduces experimental non–small-cell lung cancer

Andrea Glasauer,[1] Laura A. Sena,[1] Lauren P. Diebold,[1] Andrew P. Mazar,[2] and Navdeep S. Chandel[1]

[1]Department of Medicine, Feinberg School of Medicine, Northwestern University, Chicago, Illinois, USA. [2]Chemistry of Life Processes Institute and Robert H. Lurie Comprehensive Cancer Center, Northwestern University, Evanston, Illinois, USA.

Approximately 85% of lung cancers are non–small-cell lung cancers (NSCLCs), which are often diagnosed at an advanced stage and associated with poor prognosis. Currently, there are very few therapies available for NSCLCs due to the recalcitrant nature of this cancer. Mutations that activate the small GTPase KRAS are found in 20% to 30% of NSCLCs. Here, we report that inhibition of superoxide dismutase 1 (SOD1) by the small molecule ATN-224 induced cell death in various NSCLC cells, including those harboring *KRAS* mutations. ATN-224–dependent SOD1 inhibition increased superoxide, which diminished enzyme activity of the antioxidant glutathione peroxidase, leading to an increase in intracellular hydrogen peroxide (H_2O_2) levels. We found that ATN-224–induced cell death was mediated through H_2O_2-dependent activation of P38 MAPK and that P38 activation led to a decrease in the antiapoptotic factor MCL1, which is often upregulated in NSCLC. Treatment with both ATN-224 and ABT-263, an inhibitor of the apoptosis regulators BCL2/BCLXL, augmented cell death. Furthermore, we demonstrate that ATN-224 reduced tumor burden in a mouse model of NSCLC. Our results indicate that antioxidant inhibition by ATN-224 has potential clinical applications as a single agent, or in combination with other drugs, for the treatment of patients with various forms of NSCLC, including *KRAS*-driven cancers.

Introduction

Lung cancer is the leading cause of cancer deaths in the United States and worldwide. Non–small-cell lung cancers (NSCLCs) represent 80% of all lung cancers and are often diagnosed at an advanced stage with poor prognosis. Adenocarcinoma, a subtype of NSCLC, is the most common form of lung cancer and is characterized by activating mutations in the *KRAS* proto-oncogene in 20% to 30% of cases and by inactivating mutations in the tumor suppressor *TP53* in 50% of cases (1).

With the goal of identifying new therapies for NSCLCs, a large-scale chemical screen recently identified a small molecule that selectively induced cell death in oncogenic *KRAS*–driven ($KRAS^{onc}$-driven) cancer cells compared with normal cells. The small molecule induced cell death by increasing intracellular ROS (2). However, the mechanism by which ROS was induced and caused cell death has not yet been established. Also, it is known that oncogenic-driven cancer cells generate increased ROS as byproducts of their augmented metabolism to promote and maintain tumorigenicity (3–5). Since high levels of ROS can induce cell death (2, 6), cancer cells adapt to ROS stress by upregulating intracellular antioxidant proteins (7–10) in order to maintain ROS levels that allow protumorigenic signaling without inducing cell death. This reliance on antioxidants potentially makes cancer cells selectively vulnerable to antioxidant inhibition, as nontransformed cells generate lower basal levels of ROS and are therefore less dependent on their detoxification. In fact, studies have shown that disabling antioxidant mechanisms triggers ROS-mediated cell death in a variety of cancer cell types (11–14).

Varmus and colleagues (15) used an unbiased small-molecule screen and identified the copper-zinc–dependent enzyme and ROS regulator superoxide dismutase 1 (SOD1) as a target for inhibitors of the growth of both *KRAS*- and *EGFR*-mutant lung adenocarcinoma cells in vitro. Furthermore, SOD1 was shown to be expressed at higher levels in lung adenocarcinomas compared with the levels seen in normal lungs (15), making it an attractive therapeutic target in lung cancer. SOD1 converts superoxide to hydrogen peroxide (H_2O_2) in the cytosol, the nucleus, and the intermembrane space of the mitochondria. Through its ubiquitous expression and activity, SOD1 maintains low levels of superoxide in the cytosol, thus protecting the cell from oxidative stress and subsequent cell death. Based on this information, SOD1 inhibition can potentially be used to induce cancer cell death. However, the signaling mechanisms by which SOD1 inhibitors cause antitumorigenic effects have not yet been elucidated, nor has their therapeutic efficacy been shown in preclinical mouse models of cancer that recapitulate human cancers.

Here, we used the small molecule ATN-224 to assess SOD1 inhibition in NSCLC cells. ATN-224 is a second-generation analog of tetrathiomolybdate and has been shown to specifically inhibit SOD1 by binding and removing copper from the active site of the enzyme. This SOD1 inhibition led to an increase in steady-state levels of superoxide. ATN-224 has been shown to induce antiangiogenic effects as well as proliferation inhibition and cell death in various cancer cells (16–18). ATN-224 has also been tested in phase 2 clinical trials involving prostate cancer patients (19, 20), however without showing an efficient drug dose-response effect, which halted further trials. Furthermore, the signaling mechanism by which ATN-224 induces antitumorigenic effects in vitro is not known, thus limiting its clinical applications and further use as a single agent or in combination therapy. Last, it remains to be established whether ATN-224 would be therapeutically efficacious in a mouse model that clinically resembles human NSCLC.

In the present study, we chose *KRAS*-driven NSCLC as a model system because of the availability of the validated $Kras^{G12D}$ *Tp53*-

Conflict of interest: Andrew Mazar is a coinventor on the patent for ATN-224, which is currently owned by Wilson Therapeutics. He holds equity in and is a consultant for Wilson Therapeutics.

Citation for this article: *J Clin Invest.* 2014;124(1):117–128. doi:10.1172/JCI71714.

deficient mouse model, which reliably recapitulates human NSCLC in pathology, disease progression, clinical outcome, and response to therapies (21, 22). Furthermore, to date, there are limited therapies targeting oncogenic *KRAS* or *KRAS/TP53*-mutant NSCLCs, making *KRAS*-driven NSCLC a relevant model system for studying cancer therapeutics. Here, we report that ATN-224–mediated SOD1 inhibition induced cell death and anchorage-independent growth impairment in a variety of NSCLC cells (*KRAS* wild-type and *KRAS* mutant). ATN-224–dependent SOD1 inhibition and the resulting increase in superoxide unexpectedly inhibited glutathione peroxidases (GPXs) and peroxiredoxins (PRXs), which are antioxidant proteins known to scavenge H_2O_2. The resulting accumulation of intracellular H_2O_2 led to P38 MAPK–mediated downregulation of the antiapoptotic factor myeloid cell leukemia 1 (MCL1) and subsequent cell death. ATN-224 also synergized with the BCL2/BCLXL inhibitor ABT-263 to augment cell death. Importantly, ATN-224 showed efficacy in the clinically relevant oncogenic $Kras^{G12D}$-driven *Tp53*-deficient mouse model of lung cancer. These results suggest that inhibition of SOD1 is a viable strategy to target NSCLCs, including those harboring *KRAS* and *KRAS/TP53* mutations, which currently lack efficient, targeted treatments. Based on our in vitro data, ATN-224 might also be efficacious in other oncogenic-driven NSCLCs. Furthermore, elucidating the pro-oxidant cell death mechanism of ATN-224 allows for a potential combination treatment with other known cancer therapeutics like ABT-263.

Results

SOD1 inhibition induces cell death and anchorage-independent growth impairment in human NSCLC cells. The copper chelator ATN-224 (Supplemental Figure 1A; supplemental material available online with this article; doi:10.1172/JCI71714DS1) specifically inhibited SOD1 enzyme activity (Figure 1A) without having an effect on other copper-dependent enzymes like cytochrome C oxidase when used at concentrations up to 100 μM (23). Indeed, ATN-224 (10 μM) did not affect mitochondrial oxygen consumption, which depends on cytochrome C oxidase, in A549 human NSCLC cells harboring oncogenic *KRAS* (Supplemental Figure 1B). We show that ATN-224 induced significant cell death of A549 and other *KRAS*-mutant NSCLC cells in a dose-dependent manner (Figure 1B and Supplemental Figure 1C). Interestingly, we observed that human NSCLC cells with wild-type *KRAS* alleles were also sensitive to ATN-224 (Supplemental Figure 1D), indicating that ATN-224–mediated cell death is not specific to *KRAS*-mutant NSCLC cells. To determine whether ATN-224 specifically targeted SOD1, we infected A549 cells with two concentrations of an adenovirus encoding SOD1. We found that increasing SOD1 expression decreased ATN-224–induced cell death (Figure 1B). Furthermore, the genetic knockdown of SOD1, using two independent shRNA oligos, phenocopied the effects of ATN-224 on cell death (Figure 1, C and D). A hallmark of transformed cells is anchorage-independent growth, which can be mimicked in vitro by soft agar colony formation. Genetic knockdown of SOD1 and pharmacological inhibition of SOD1 by ATN-224 impaired the anchorage-independent growth ability of A549 cells (Figure 1, E and F). We found that SOD1 inhibition only mildly affected the cell viability of differentiated normal bronchial epithelial cells (NBECs) (Figure 1, G and H). Taken together, SOD1 inhibition reduced the transforming potential of a variety of NSCLC cells in vitro, while minimally affecting their nontransformed counterparts, NBECs.

SOD1 inhibition induces cell death by diminishing antioxidant protein activities, leading to increased intracellular H_2O_2. To investigate the mechanism by which ATN-224–mediated SOD1 inhibition induced the death of NSCLC cells, we determined the intracellular superoxide and H_2O_2 levels by oxidation of dihydroethidium (DHE) and 2′,7′-dichlorodihydrofluorescein (DCFH), respectively. As expected, ATN-224 increased superoxide levels in A549 cells (Supplemental Figure 2A). Surprisingly, ATN-224 also induced a significant increase in H_2O_2 levels that was reverted by the addition of Mn(III)tetrakis(4-benzoic acid) porphyrin (MnTBAP), a SOD mimetic with catalase-like activity (Figure 2A) that is insensitive to copper chelation by ATN-224. The ATN-224–mediated increase in H_2O_2 was verified by using a redox-sensitive GFP (roGFP) probe and roGFP2 linked to a thiol peroxidase (ORP1), which increase sensitivity to H_2O_2 (ref. 24 and Figure 2B and C). In addition to decreasing oxidative stress, we found that MnTBAP abrogated ATN-224–induced cell death and anchorage-independent growth impairment in A549 and H460 $KRAS^{onc}$ human NSCLC cells (Figure 2, D and E, and Supplemental Figure 2, B and C). Therefore, ATN-224 appears to increase both superoxide and H_2O_2, which leads to lung cancer cell death. Exogenous superoxide, produced by adding xanthine and xanthine oxidase to the cell culture media, also induced cell death in A549 cells (Supplemental Figure 2D).

SOD1 is the primary enzyme-converting superoxide into H_2O_2. Therefore, our findings were initially surprising because H_2O_2 was expected to decrease, not increase, upon SOD1 inhibition. To investigate our paradoxical finding of how H_2O_2 could increase upon inhibition of the H_2O_2 generator SOD1, we first examined SOD1 protein expression. Because SOD1 protein levels were not elevated by ATN-224 (Figure 2F), we next wanted to assess whether ATN-224–mediated SOD1 inhibition affected the activity of enzymes that metabolize H_2O_2. GPXs convert H_2O_2 into water (25). Interestingly, Fridovich and colleagues previously showed that GPXs are inactivated by superoxide radicals (26), leading to an increase in H_2O_2. Given that superoxide radicals are increased upon ATN-224 treatment (Supplemental Figure 2A), we tested the effect of ATN-224 on GPXs and found that GPX enzyme activity was significantly decreased upon drug treatment (Figure 2G). We observed that the GPX mimetic ebselen and the antioxidant glutathione (GSH) precursor N-acetyl cysteine (NAC), which metabolize H_2O_2, rescued ATN-224–induced cell death and anchorage-independent growth impairment in A549 cells (Figure 2, H and I, and Supplemental Figure 2E), suggesting that increased levels of H_2O_2 are required for ATN-224–dependent cell death. We found that ebselen also dampened the ATN-224–mediated increase in H_2O_2 levels (Figure 2A). To further support our findings, adenoviral overexpression of GPX1 abrogated ATN-224–induced cell death in A549 cells (Figure 2J). PRXs are another family of antioxidant proteins that scavenge physiological levels of H_2O_2. However, under high H_2O_2 stress, PRXs are susceptible to H_2O_2-mediated hyperoxidation, resulting in their inactivation (25). Here, we found that in addition to diminishing GPX enzyme activity, ATN-224 led to the inhibition of PRXs. We measured PRX oxidation and inhibition using an antibody specific to the inactive sulfinic and sulfonic forms of PRX 1 to 4 (PRX-SO_3). PRX inhibition was prevented by the antioxidants MnTBAP and ebselen (Figure 2K). Collectively, our data suggest that ATN-224–induced cancer cell death is mediated through the inhibition of the antioxidant GPX proteins, resulting in an increase in intracellular H_2O_2. Elevated H_2O_2 levels then oxidize and inactivate PRXs, which further increases H_2O_2 and drives cell death.

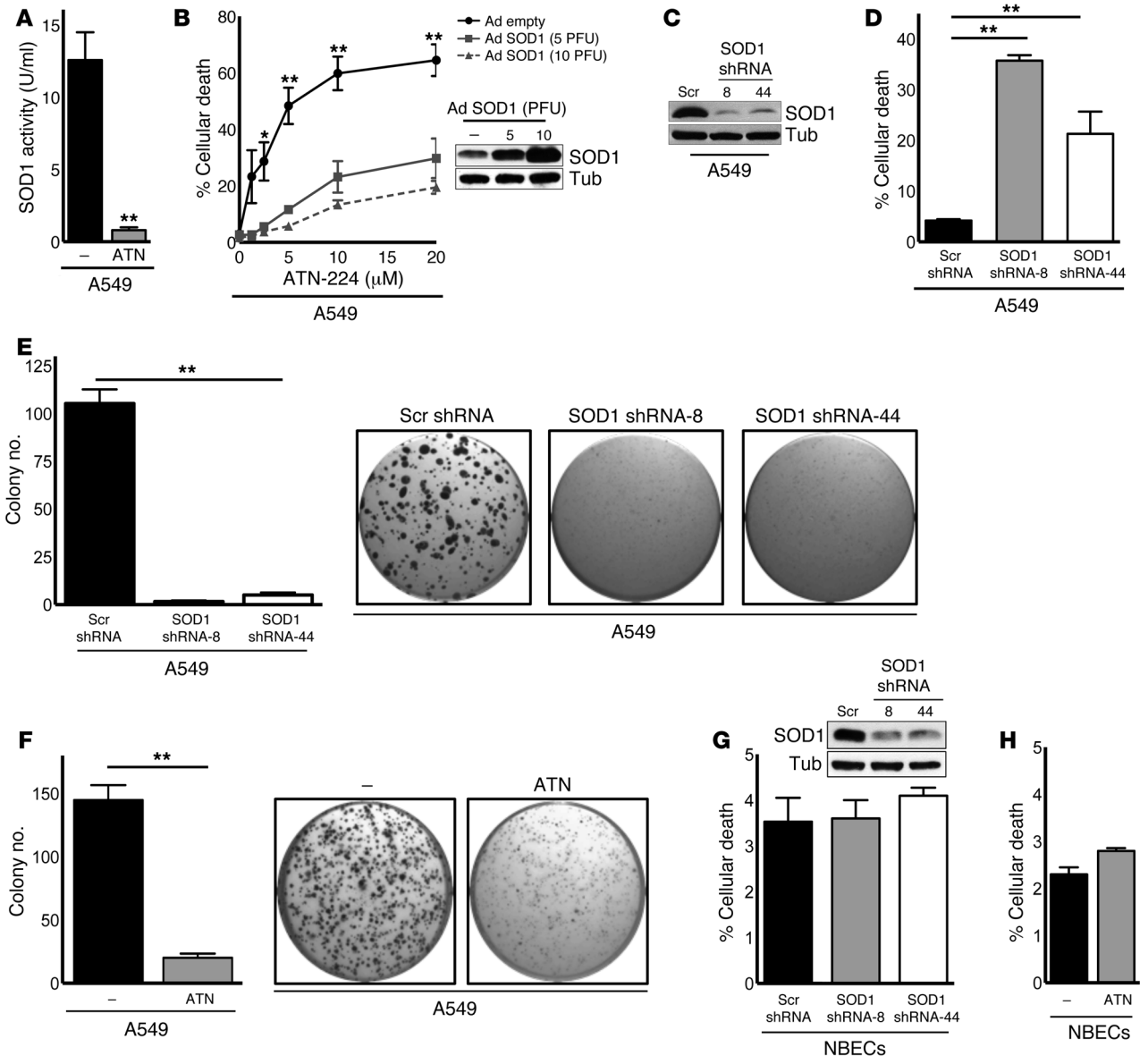

Figure 1

SOD1 inhibition causes cell death and anchorage-independent growth impairment in human NSCLC cells. (**A**) SOD1 activity assay of A549 *KRAS*^{onc} human NSCLC cells treated for 24 hours with 10 μM ATN-224 (n = 3). (**B**) A549 cells expressing an empty adenoviral control vector or adenoviral SOD1 (Ad SOD1) were treated with increasing doses of ATN-224 (1.25, 2.5, 5, 10, and 20 μM), and cell death (96 hours) was determined (n = 3). Immunoblot for SOD1 of empty or Ad SOD1–expressing cells. Tubulin (Tub) was used as a loading control. (**C** and **D**) A549 cells expressing a pLKO.1 lentiviral scrambled (Scr) control vector or two independent SOD1 shRNA vectors (clones 8 and 44) were (**C**) immunoblotted for SOD1 and (**D**) analyzed for cell death 96 hours after infection (n = 3). (**E** and **F**) Analysis of soft agar colonies of A549 cells (**E**) expressing pLKO.1 control or SOD1 shRNA vectors (clones 8 and 44) and (**F**) treated for 3 weeks with 10 μM ATN-224. Images show colony formation in 96-well plates (n = 8, n = 13). (**G** and **H**) NBECs (**G**) expressing pLKO.1 control or SOD1 shRNA vectors (clones 8 and 44) were immunoblotted for SOD1 or (**H**) treated with 10 μM ATN-224 and analyzed for cell death (96 hours) (n = 3). Data are represented as the mean ± SEM. *P < 0.05. **P < 0.01. See also Supplemental Figure 1.

ATN-224–induced H_2O_2 downregulates MCL1, leading to BIM/PUMA-mediated programmed cell death. Next, we wanted to investigate how the increase in H_2O_2 levels caused by SOD1 inhibition induced cell death. A549 cells were treated with the caspase inhibitor zVAD, which protected cells from ATN-224–mediated cell death (Figure 3A). Furthermore, we found that ATN-224 induced cleaved caspase 3 (CC3) protein expression (Figure 3B), indicating that SOD1 inhibition induced caspase-dependent programmed cell death. Proapoptotic B cell lymphoma 2 (BCL2) proteins BAX and BAK induce programmed cell death through caspase 9 (27). Here, we observed that immortalized *Casp9*$^{-/-}$ and *Bax*$^{-/-}$*Bak*$^{-/-}$ mouse embryonic fibroblasts (MEFs) were protected against ATN-224–induced cell death compared with wild-type MEFs, indicating that ATN-224 induces cell death through the intrinsic (mitochondrial)

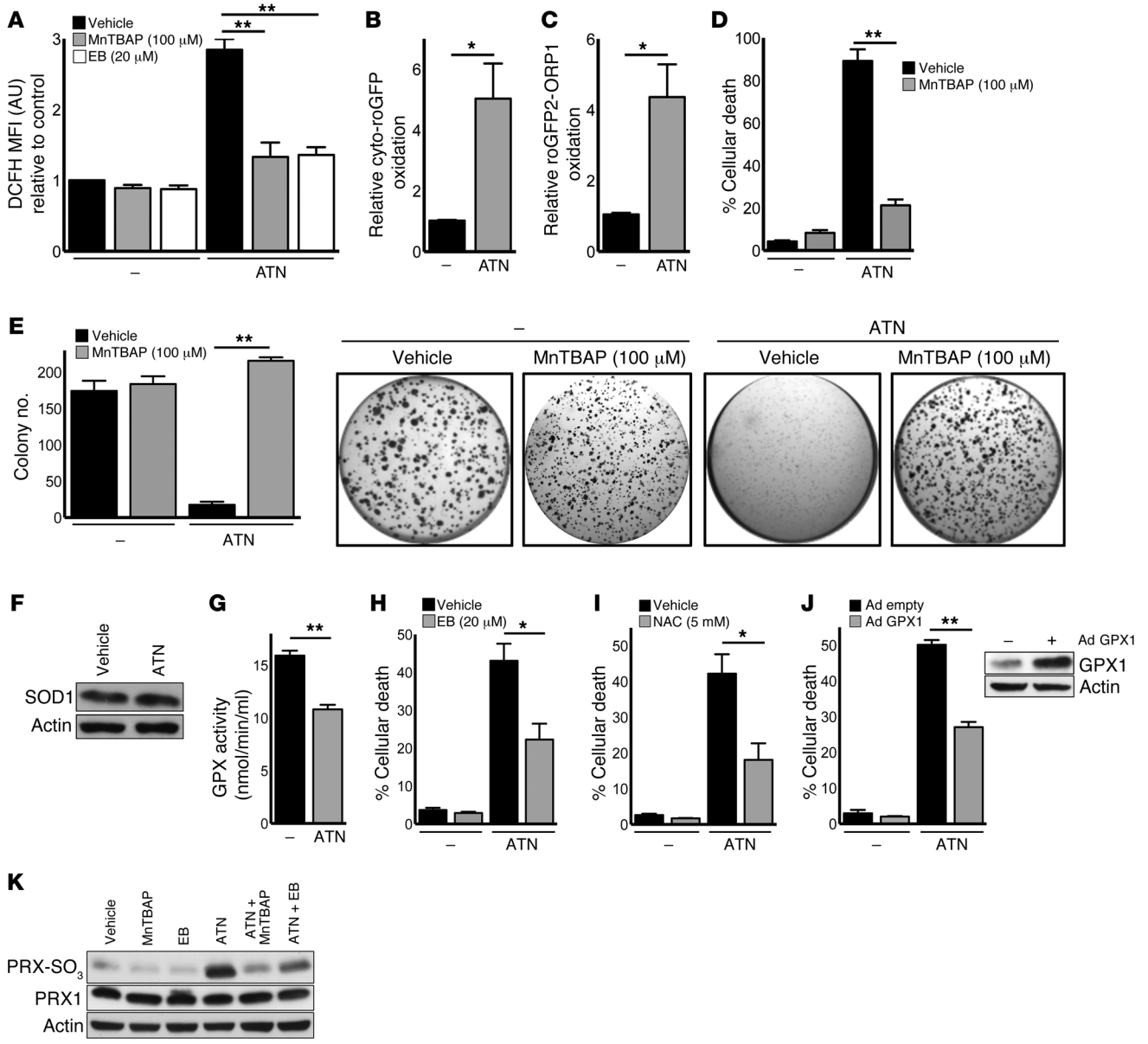

Figure 2

SOD1 inhibition induces cell death by diminishing antioxidant protein activities, leading to an increase in H_2O_2. (**A**) A549 cells were treated with 10 μM ATN-224 alone or with 100 μM MnTBAP or 20 μM ebselen. ROS levels were determined by DCFH staining (10 μM, 24 hours) (n = 3). (**B** and **C**) A549 cells were treated with 10 μM ATN-224, and H_2O_2 levels were determined by (**B**) cyto-roGFP or (**C**) roGFP2-ORP1 oxidation (both 24 hours) (n = 3). (**D** and **E**) A549 cells were treated with 10 μM ATN-224 alone or with 100 μM MnTBAP, and (**D**) cell death (96 hours) and (**E**) anchorage-independent growth (3 weeks) were determined (n = 3, n = 7). (**F**) ATN-224–treated A549 cell lysates were taken (48 hours) and immunoblotted for SOD1. (**G**) A549 cells were treated with 10 μM ATN-224, and GPX activity was determined (48 hours) (n = 4). (**H** and **I**) A549 cells were treated with 10 μM ATN-224 alone or with (**H**) 20 μM ebselen or (**I**) 5 mM NAC, and cell death was determined (96 hours) (n = 4, n = 3). (**J**) A549 cells expressing empty adenoviral vector (Ad empty) or adenoviral GPX1 (Ad GPX1) were treated with 10 μM ATN-224, and cell death (96 hours) was determined (n = 7). Immunoblot for GPX1. (**K**) A549 cells were treated with 10 μM ATN-224 alone or with 100 μM MnTBAP or 20 μM ebselen. Cell lysates were immunoblotted for PRX-SO_3. PRX1 was used as a loading control. Data are represented as the mean ± SEM. *P < 0.05. **P < 0.01. See also Supplemental Figure 2.

death pathway (Figure 3, C and D). Proapoptotic BH3-only proteins including BIM, PUMA, and NOXA trigger apoptosis through the activation of BAX and BAK. To test which BH3-only proteins are required for ATN-224–mediated cell death, we drug-treated immortalized *Puma*$^{-/-}$, *Bim*$^{-/-}$, and *Noxa*$^{-/-}$ knockout MEFs. *Bim*$^{-/-}$ *Puma*$^{-/-}$ double-knockout MEFs were protected against ATN-224–induced cell death compared with wild-type MEFs (Figure 3E). The individual loss of PUMA, BIM, or NOXA was not sufficient to protect against ATN-224 (Supplemental Figure 3, A–C). Antiapoptotic BCL2 proteins including BCLXL and MCL1 prevent BAX/

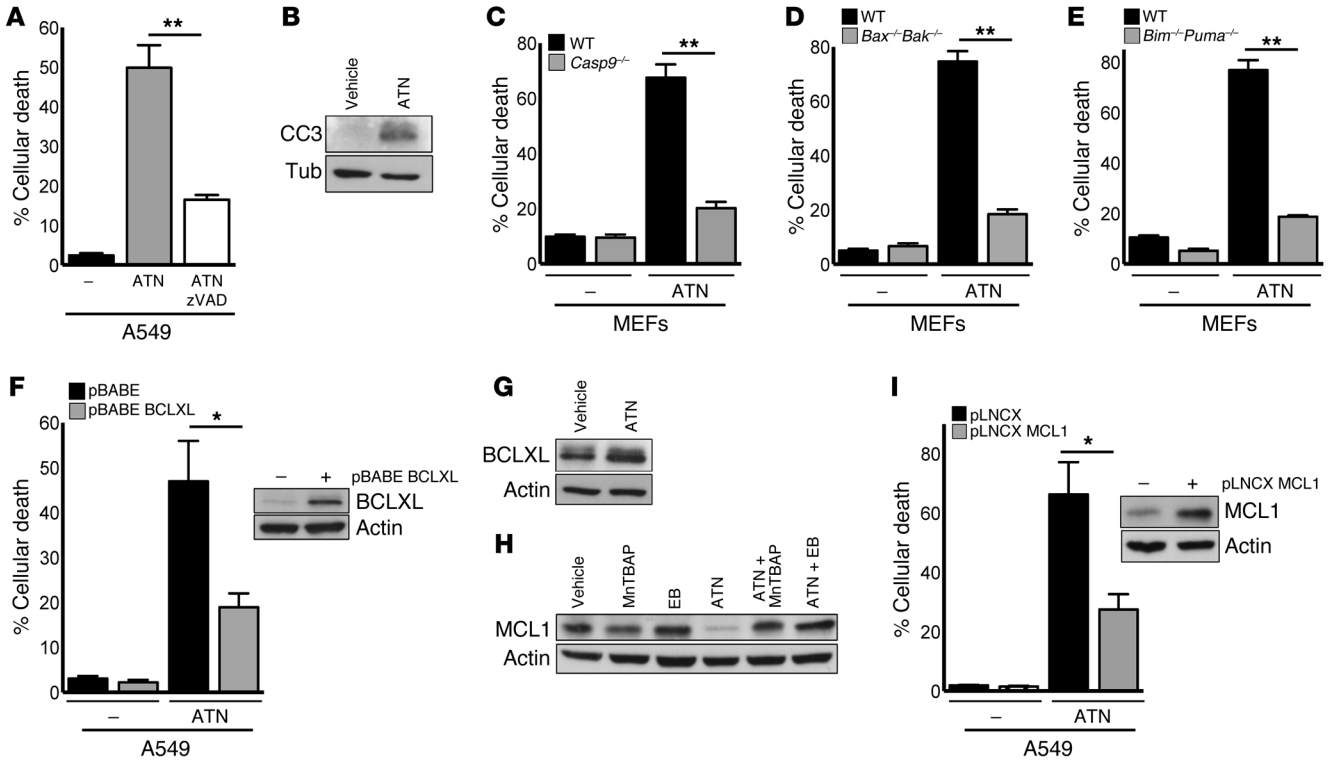

Figure 3

ATN-224–induced H_2O_2 downregulates MCL1 protein expression, leading to programmed cell death. (**A**) A549 cells were treated with 10 μM ATN-224 alone or with 30 μM caspase inhibitor zVAD, and cell death (96 hours) was determined ($n = 3$). (**B**) A549 cells were treated with 10 μM ATN-224. Cell lysates (72 hours) were immunoblotted for CC3. (**C**–**E**) Immortalized wild-type or (**C**) *Casp9*$^{-/-}$ MEFs, (**D**) *Bax*$^{-/-}$*Bak*$^{-/-}$ MEFs, and (**E**) *Bim*$^{-/-}$*Puma*$^{-/-}$ MEFs were treated with 5 μM ATN-224, and cell death (48 hours) was determined (all $n = 3$). (**F**) A549 cells expressing a pBABE control or BCLXL vector were treated with 10 μM ATN-224, and cell death (96 hours) was determined ($n = 4$). Immunoblot for BCLXL of control or BCLXL vector–expressing cells. (**G**) A549 cells were treated with 10 μM ATN-224, and lysates (48 hours) were immunoblotted for BCLXL. (**H**) A549 cells were treated with 10 μM ATN-224 alone or with 100 μM MnTBAP or 20 μM ebselen. Lysates (48 hours) were immunoblotted for MCL1. (**I**) A549 cells expressing a pLNCX control or MCL1 vector were treated with 10 μM ATN-224, and cell death (96 hours) was determined ($n = 3$). Immunoblot for MCL1 of control or MCL1 vector–expressing cells. Data are represented as the mean ± SEM. *$P < 0.05$. **$P < 0.01$. See also Supplemental Figure 3.

BAK activation. A549 cells retrovirally expressing the antiapoptotic factors BCLXL and MCL1 were protected against ATN-224–induced cell death compared with cells expressing a control vector (Figure 3, F and I). BCLXL protein levels were not affected by ATN-224 (Figure 3G), however ATN-224 greatly decreased MCL1 protein expression, an effect that was reverted by the addition of the antioxidants MnTBAP and ebselen (Figure 3H). These findings suggest that the ATN-224–induced increase in H_2O_2 triggers NSCLC cell death through the activation of proapoptotic BH3-only proteins BIM and PUMA and the downregulation of the antiapoptotic protein MCL1. MCL1 is highly expressed in a variety of cancers, including NSCLCs (28, 29), and has been associated with resistance to cancer therapies (30, 31).

ATN-224–induced H_2O_2 activates P38 MAPK signaling, leading to MCL1 downregulation and cell death. Previous studies have shown that H_2O_2 can trigger MAPK-induced cell death through the stress-activated kinases c-Jun N-terminal kinase (JNK) and P38 (6). P38 MAPK has been established as a tumor suppressor and ROS sensor in tumorigenesis (32). Furthermore, JNK and P38 MAPKs have MCL1 degron consensus sites and have been implicated in MCL1 inactivation and protein decline upon oxidative stress (33). To determine whether MAPKs mediate ATN-224–induced MCL1 downregulation and subsequent cell death, we drug-treated A549 cells and analyzed them for signaling pathway activity. ATN-224 induced phosphorylation and therefore activation of P38 MAPK (Figure 4A), while JNK and extracellular signal–regulated kinases 1/2 (ERK1/2) were not affected by ATN-224 (Figure 4, C and D). The antioxidants ebselen and MnTBAP attenuated P38 MAPK phosphorylation, indicating that this kinase is dependent on H_2O_2 for activation (Figure 4A). To confirm that ATN-224 activates only P38 MAPK signaling and subsequent cell death, we treated A549 cells with P38 MAPK, JNK, or ERK1/2 inhibitors. We found that only the P38 MAPK inhibitor SB203580 (called SB) protected against ATN-224–induced cell death (Figure 4, B–D). Inhibition of P38 MAPK also prevented the activation of its well-defined target MAPK-activated protein kinase 2 (MAPKAPK-2) and, more importantly, rescued MCL1 protein expression in the presence of ATN-224 (Figure 4, E and F). These results indicate that ATN-224–mediated SOD1 inhibition and the resulting increase in H_2O_2 activate P38 MAPK signaling, leading to a decline in MCL1 protein expression and cell death.

ATN-224 triggers cell death in oncogenic Kras^{G12D} Tp53-deficient mouse lung adenocarcinoma cells. In addition to *KRAS* mutations, 50% of

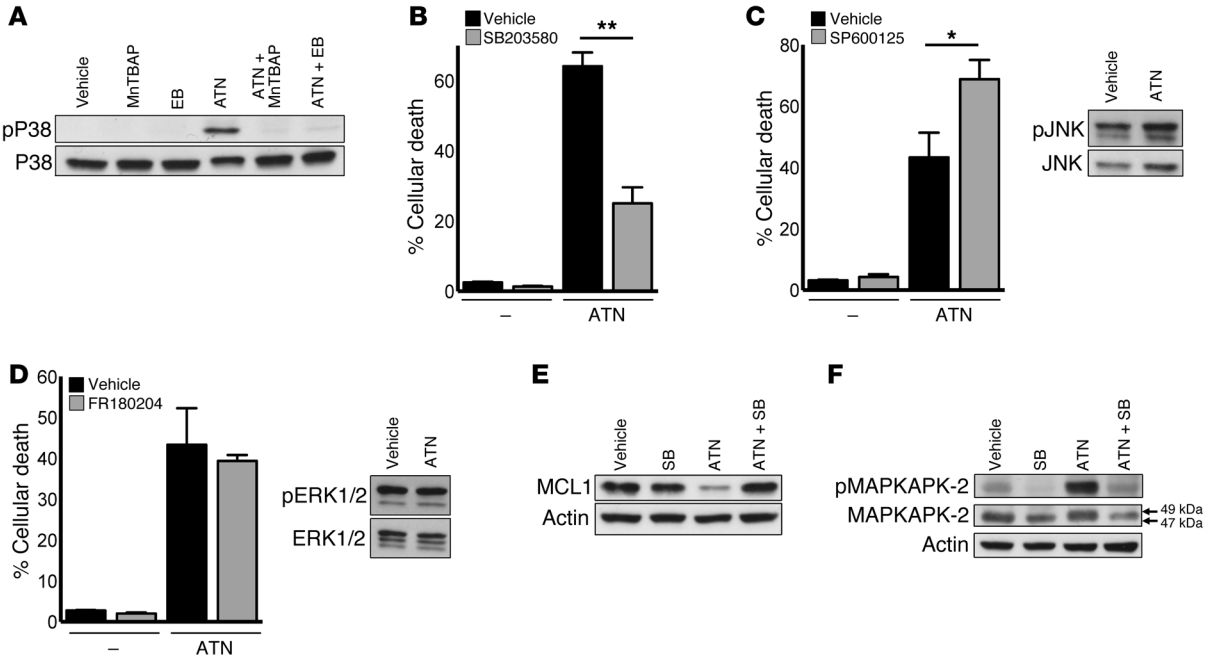

Figure 4

ATN-224–mediated increase in H_2O_2 activates P38 MAPK activity, leading to MCL1 downregulation and cell death. (**A**) A549 cells were treated with 10 μM ATN-224 alone or with 100 μM MnTBAP or 20 μM ebselen. Lysates (48 hours) were immunoblotted for phospho(Thr180/Tyr182)-P38 MAPK. Total P38 MAPK was used as a loading control. (**B**) A549 cells were treated with 10 μM ATN-224 alone or with 10 μM of the P38 inhibitor SB203580, and cell death (96 hours) was determined ($n = 9$). (**C** and **D**) A549 cells were treated with 10 μM ATN-224 alone or with either (**C**) 10 μM of the JNK inhibitor SP600125 or (**D**) 2.5 μM of the ERK1/2 inhibitor FR180204. Cell death (96 hours) was determined ($n = 4$, $n = 3$). Vehicle and ATN-224 cell lysates (48 hours) were immunoblotted for (**C**) phospho(Thr183/Tyr185) JNK or (**D**) phospho(Thr202/Tyr204) ERK1/2. Total JNK and total ERK1/2 were used as loading controls. (**E** and **F**) A549 cells were treated with 10 μM ATN-224 alone or with 10 μM of the P38 MAPK inhibitor SB203580. Lysates (48 hours) were immunoblotted for (**E**) MCL1 or (**F**) the P38 MAPK target phospho(Thr222)-MAPKAPK-2. Shift of total MAPKAPK-2 (**F**) to 49 kDa indicates phosphorylation. Data are represented as the mean ± SEM. $^*P < 0.05$. $^{**}P < 0.01$.

NSCLC cases show inactivating mutations in the tumor suppressor gene *TP53* (1). To test whether ATN-224 can induce cell death in oncogenic *KRAS/TP53*-mutant cancer cells, we used genetically defined mouse lung adenocarcinoma cells from tumors carrying a Cre-inducible oncogenic $Kras^{G12D}$ allele (*LSL-*$Kras^{G12D/+}$) and a conditional loss-of-function *Tp53* allele ($Tp53^{fl/fl}$) (referred to hereafter as KP cells). Corroborating our human $KRAS^{onc}$ NSCLC data, ATN-224 induced dose-dependent cell death in KP cells (Figure 5A). Cell death was abrogated by the addition of the antioxidant MnTBAP and the GPX mimetic ebselen in KP cells (Figure 5B). Furthermore, we found that P53 inhibition did not rescue ATN-224–induced cell death in A549 cells (Supplemental Figure 4A), suggesting that P53 is not required for ATN-224–dependent cell death. ATN-224 also impaired the anchorage-independent growth ability of KP cells in soft agar, which was recovered by MnTBAP (Figure 5C). We investigated the signaling mechanism by which SOD1 inhibition induced cell death in KP cells and found that ATN-224 led to a decline in protein expression of the antiapoptotic factor MCL1 and an upregulation of activated phospho-P38 MAPK, both of which were reversed by the addition of MnTBAP or ebselen (Figure 5D). Supporting these data, we found that P38 MAPK inhibition with SB203580 rescued ATN-224–induced cell death (Figure 5E). Together, our findings indicate that ATN-224–induced SOD1 inhibition diminished the transforming potential of oncogenic $Kras^{G12D}$ *Tp53*-deficient lung cancer cells in vitro.

ATN-224 reduces tumor burden in a clinically relevant $Kras^{G12D}$ *Tp53-deficient mouse model of lung cancer.* To address whether ATN-224–induced SOD1 inhibition is efficient at reducing lung cancer in vivo, we crossed *LSL-*$Kras^{G12D/+}$ mice (22) with mice harboring floxed alleles of *Tp53* (hereafter termed KP mice). Upon intratracheal administration of adenoviral-Cre recombinase (adeno-Cre), the *Kras* oncogene is activated and *Tp53* is knocked out in the mouse lung. KP mice rapidly develop tumors that resemble human lung adenocarcinoma and have been shown to respond to known therapies of NSCLC similarly to human tumors (21). To test the efficacy of ATN-224 in KP tumors, we intratracheally infected 6- to 10-week-old KP mice with adeno-Cre. Eight weeks postinfection (8 wpi), mice were treated with 4 mg/kg ATN-224 or PBS by i.p. injections every other day for 4 weeks (Figure 6A). ATN-224 was well tolerated, and no mortalities or treatment-related effects on the clinical signs or body weights of the treated mice were observed during the 4-week treatment period (data not shown). Mice showed lung tumor formation 8 wpi, making the drug treatment clinically relevant (Supplemental Figure 5A). We tested three independent cohorts of mice (5–6 mice per cohort per condition) and found that ATN-224 accumulated in the blood plasma of the drug-treated mice at a therapeutic level (Figure 6B). Furthermore, ATN-224 decreased lung weight, normalized to animal body weight (Figure 6C). We performed histological analysis using H&E staining of KP lung sections, which showed a significant decrease in lesion num-

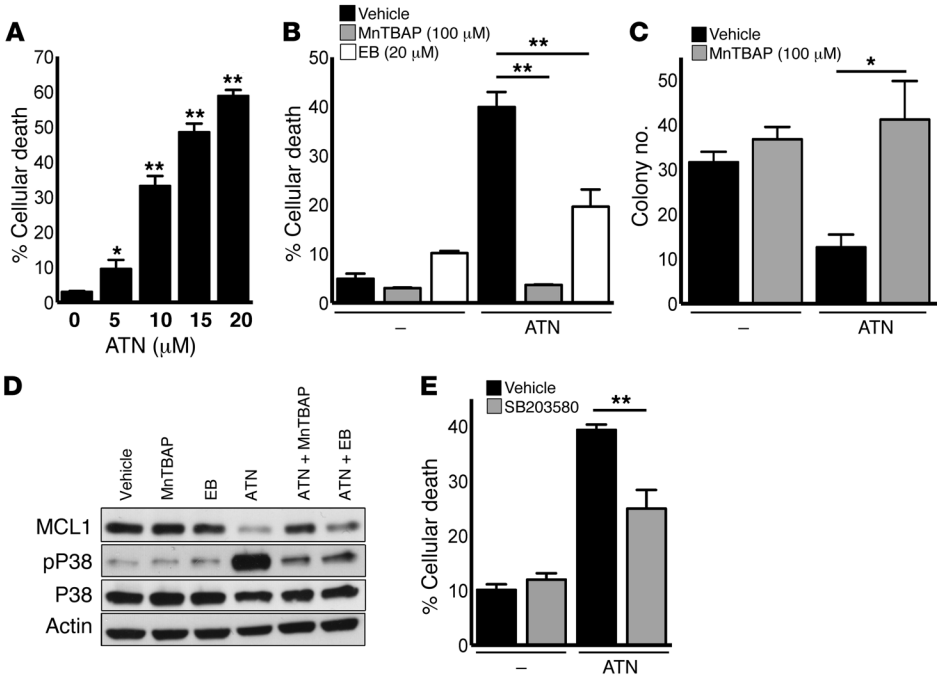

Figure 5

ATN-224–mediated SOD1 inhibition induces cell death in *Kras*^{G12D} *Tp53*$^{fl/fl}$–driven mouse lung cancer cells. (**A**) KP cells were treated with increasing doses of ATN-224 (5, 10, 15, and 20 μM), and cell death (96 hours) by trypan blue staining was determined (n = 4). Statistical significance was determined by comparing 0 μM ATN-224 with increasing concentrations. (**B**) KP cells were treated with 15 μM ATN-224 alone or with 100 μM MnTBAP or 20 μM ebselen, and cell death (96 hours) was determined (n = 3). (**C**) Analysis of soft agar colonies of KP cells treated with 10 μM ATN-224 alone or with 100 μM MnTBAP (3 weeks) (n = 5). (**D**) KP cells were treated with 15 μM ATN-224 alone or with 100 μM MnTBAP or 20 μM ebselen. Lysates (48 hours) were immunoblotted for phospho-P38 MAPK (pP38) and MCL1. Total P38 MAPK was used as a loading control. (**E**) KP cells were treated with 15 μM ATN-224 alone or with 10 μM of the P38 MAPK inhibitor SB203580. Cell death (96 hours) was determined (n = 4). Data are represented as the mean ± SEM. *P < 0.05. **P < 0.01. See also Supplemental Figure 4.

bers and overall tumor burden in KP lungs from mice treated with ATN-224 compared with those treated with PBS (Figure 6, D, E, and H). To address whether ATN-224 impaired cell proliferation and induced cell death, we stained PBS- and ATN-224–treated KP lung sections for KI67, an index for proliferation, and for CC3, a marker of apoptotic cells. Tumors from ATN-224–treated KP mice displayed a decreased number of KI67-positive cells and an increase in CC3-positive cells (Figure 6, F–H). Thus, ATN-224 as a single agent is efficient at reducing tumor burden in a preclinical *Kras*^{G12D}-driven mouse model of lung cancer that also harbors a *Tp53* loss-of-function mutation, which is often a predictor of poor prognosis.

ATN-224 synergizes with proapoptotic and pro-oxidant drugs to induce augmented cell death in NSCLC cells. Our data show that ATN-224 has substantial efficacy as a single agent against NSCLC, including oncogenic *KRAS* and *KRAS/TP53*-driven lung cancer in vitro and in vivo. Having established the pro-oxidant mechanism by which ATN-224 induces cancer cell death, we next wanted to test whether the efficacy of ATN-224 could be enhanced by synergy with other therapeutic agents, based on their mechanism of action. ATN-224 specifically downregulated the antiapoptotic factor MCL1 (Figure 3H and Figure 5D). BCL2 and BCLXL are also antiapoptotic proteins acting independently of MCL1 through the binding and inhibition of BAX and BAK. The orally available BH3 mimetic ABT-263 (navitoclax) is a BCL2/BCLXL inhibitor and is currently in clinical trials for small-cell lung cancer and B cell malignancies (34). Because ATN-224 and ABT-263 both target independent antiapoptotic BCL2 family members, we tested whether these small molecules synergize in NSCLC cells. KP mouse, A549, and H460 cells treated with a combination of ATN-224 and ABT-263 showed an increase in cell death compared with cells treated with ATN-224 alone (Figure 7, A–C). We also found that ATN-224 diminished GPX enzyme activities in order to increase H_2O_2 levels (Figure 2), which potentially would make cells susceptible to other agents that further diminish GPX activity. Buthionine sulphoximine (BSO) depletes the reduced form of the antioxidant GSH, which is required for GPX activity (35). BSO exhibited anticancer activity through apoptosis as a single agent in solid tumors (36). As with ABT-263, we observed that KP mouse, A549, and H460 cells treated with a combination of the pro-oxidant drugs ATN-224 and BSO showed an increase in cell death compared with cells treated with ATN-224 alone (Figure 7, D–F). The combination of ATN-224 with either ABT-263 or BSO still induced cell death through BAX/BAK activation (Figure 7, G and H). Our data indicate that ATN-224, in addition to its function as a single agent, may have therapeutic benefits in combination treatments with other proapoptotic and pro-oxidant drugs in NSCLCs.

Discussion

Research studies and clinical trials have shown that targeted cancer therapeutics are successfully used in a subset of patients with NSCLC (37). However, no effective targeted therapies are currently available for oncogenic *KRAS*-induced lung cancer. In this study, we found that, in addition to causing cell death in a variety of *KRAS*-mutant and *KRAS* wild-type human NSCLC cells, the SOD1 inhibitor ATN-224 had substantial antitumor activity as a single agent in a preclinical mouse model of lung cancer bearing oncogenic *Kras*^{G12D} and *Tp53* loss-of-function mutations when administered 8 weeks after tumor initiation. Consistent with our findings, Varmus and colleagues identified SOD1 as a promising lung cancer therapeutic target in a screen for inhibitors of lung adenocarcinoma cell growth (oncogenic *KRAS*– and *EGFR*–driven) and furthermore showed that most human lung adenocarcinomas express SOD1 at higher-than-normal levels (15). Importantly, SOD1 inhibition has the potential to selectively kill cancer cells. Our data in NBECs (Figure 1, G and H) show that targeting SOD1 selectively induced cancer cell death by exploiting their vulnerability to damage by further ROS insult without causing substantial

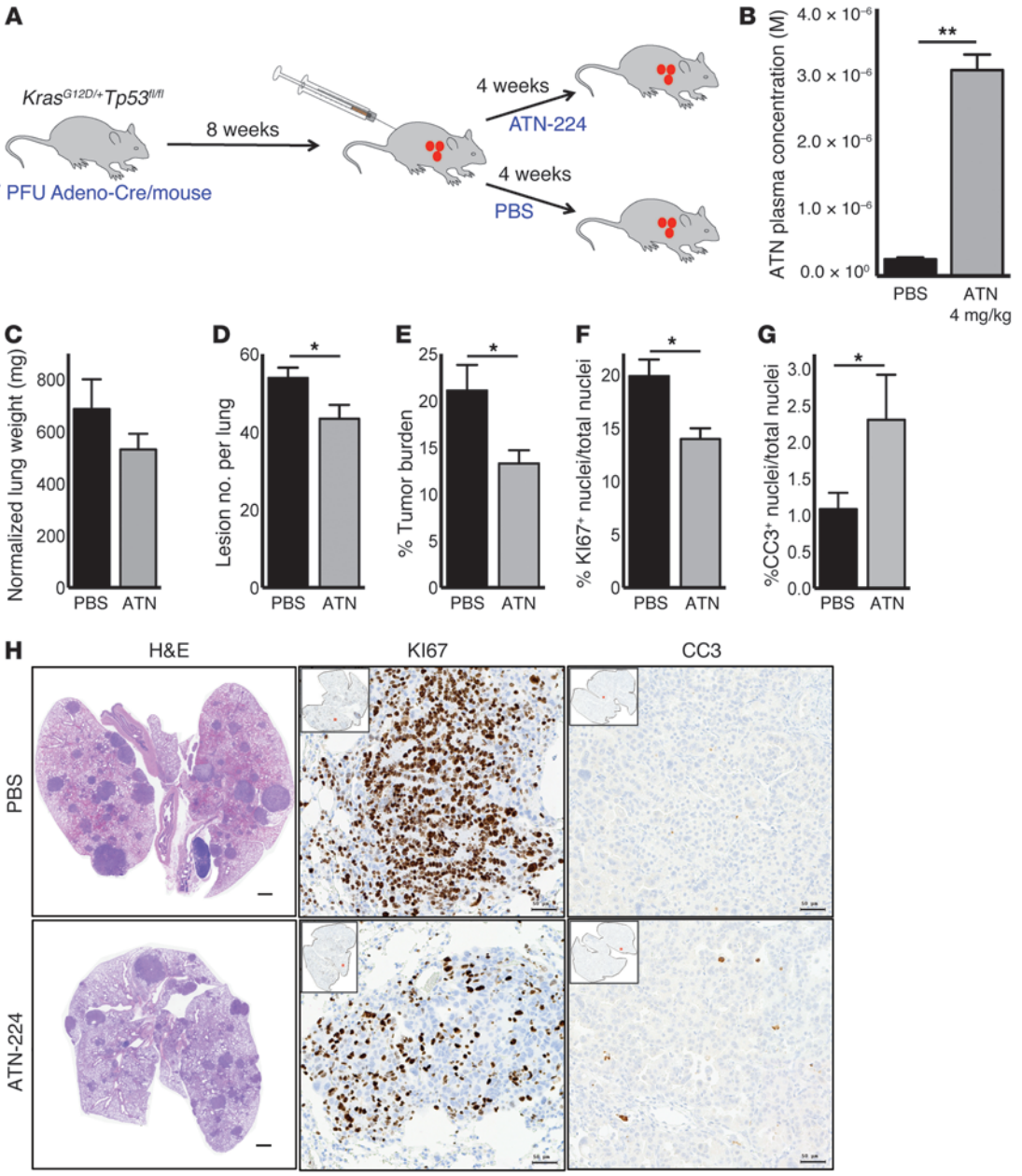

Figure 6

ATN-224 as a single agent reduces tumor burden in a preclinical *Kras*^{G12D} *Tp53*$^{fl/fl}$–driven mouse model of lung cancer. (**A**) Schematic of experimental design. KP mice were intubated with 10^7 PFUs of adenoviral Cre and treated 8 wpi with PBS or 4 mg/kg ATN-224 every 2 days for 4 weeks. (**B**) KP mice were injected i.p. with PBS or 4 mg/kg ATN-224 for 4 weeks, and ATN-224 levels in blood plasma were determined (n = 3). (**C**–**E**) Lungs isolated from PBS and ATN-224–treated KP mice were analyzed for (**C**) lung weight normalized to body weight, (**D**) number of lesions per whole lung section, and (**E**) tumor burden per whole lung section (n = 16 PBS, n = 17 ATN-224). Tumor burden was calculated by averaging the tumor area from H&E-stained whole lung sections shown in **H** (left panel). (**F** and **G**) Lungs isolated from PBS and ATN-224–treated KP mice were analyzed for (**F**) KI67-positive cells per lung section and (**G**) CC3-positive cells per lung section (n = 5 PBS, n = 5 ATN-224). (**H**) Representative images of H&E- (left panels), KI67- (middle panels), and CC3-stained (right panels) KP lung sections from PBS and ATN-224–treated mice. H&E-stained images of whole lung sections represent tumor burden. Scale bars: 1 mm (left panels). KI67 (proliferation) and CC3 (cell death) images of tumors; positively stained cells appear in brown and nuclei in blue. Scale bars: 50 μM (middle and right panels). Data are represented as the mean ± SEM. *P < 0.05. **P < 0.01. See also Supplemental Figure 5.

stress to normal cells with lower basal levels of ROS. The SOD1 inhibitor ATN-224 specifically has been tested in phase 1 clinical trials in patients with solid tumors and hematological malignancies (38, 39) and in phase 2 clinical trials for prostate cancer (19, 20). Our results suggest that ATN-224, as a single agent or in combination therapy, might have therapeutic utility in patients with various oncogenic-driven NSCLCs, including patients harboring oncogenic *KRAS* or *KRAS/TP53* mutations.

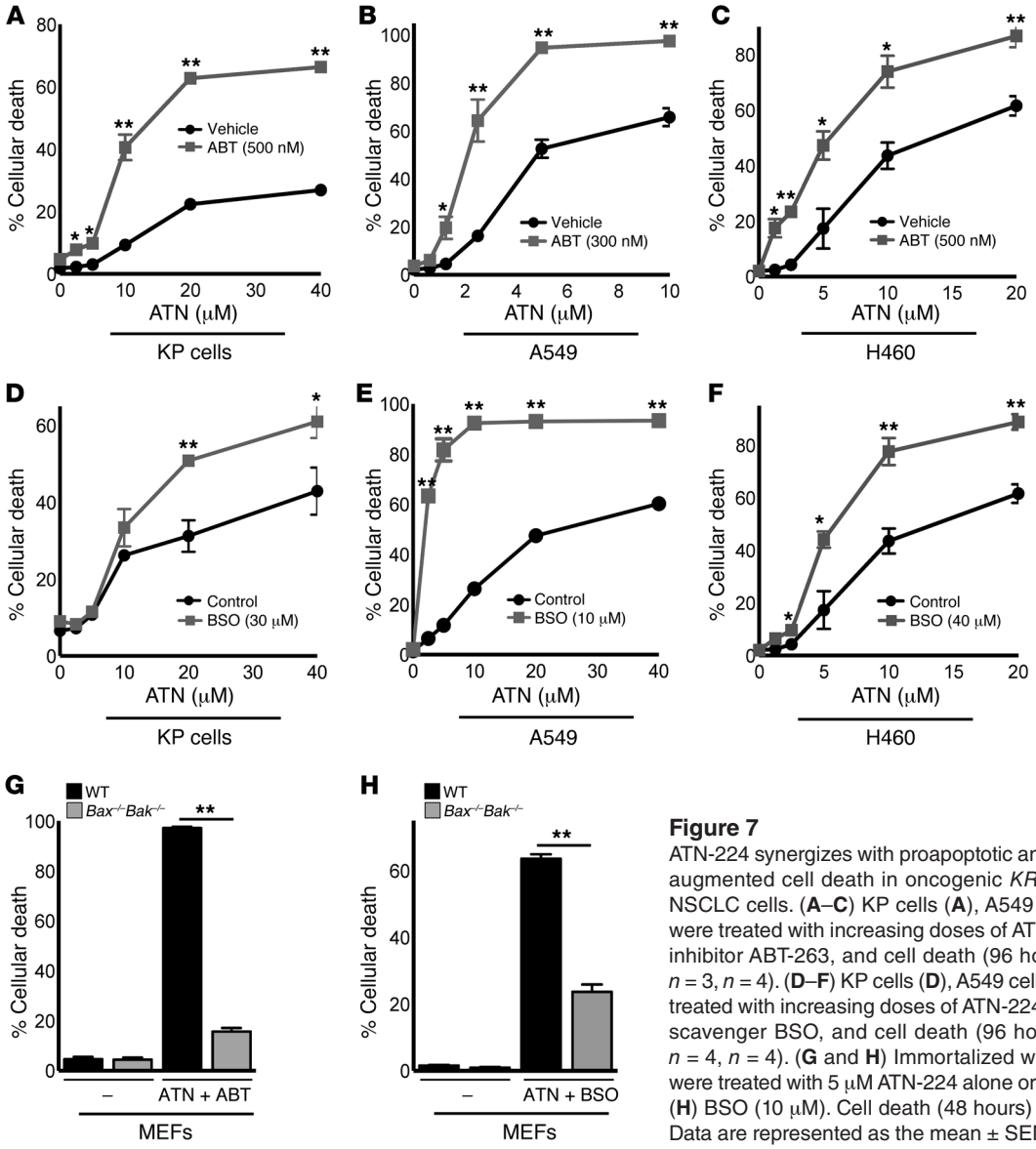

Figure 7

ATN-224 synergizes with proapoptotic and pro-oxidant drugs to induce augmented cell death in oncogenic *KRAS*– and *KRAS*/*TP53*-driven NSCLC cells. (**A**–**C**) KP cells (**A**), A549 cells (**B**), and H460 cells (**C**) were treated with increasing doses of ATN-224 alone or with the BCL2 inhibitor ABT-263, and cell death (96 hours) was determined ($n = 4$, $n = 3$, $n = 4$). (**D**–**F**) KP cells (**D**), A549 cells (**E**), and H460 cells (**F**) were treated with increasing doses of ATN-224 alone or with the glutathione scavenger BSO, and cell death (96 hours) was determined ($n = 4$, $n = 4$, $n = 4$). (**G** and **H**) Immortalized wild-type or *Bax*$^{-/-}$*Bak*$^{-/-}$ MEFs were treated with 5 μM ATN-224 alone or with (**G**) ABT-263 (300 nM) or (**H**) BSO (10 μM). Cell death (48 hours) was determined (both $n = 3$). Data are represented as the mean ± SEM. $^{*}P < 0.05$. $^{**}P < 0.01$.

The signaling mechanisms by which SOD1 inhibition and subsequent changes in ROS levels cause cell death and antitumorigenic effects have not yet been elucidated. Here, we found H_2O_2 to be the major signaling oxidant responsible for ATN-224–induced NSCLC cell death and reduction in tumorigenicity (Supplemental Figure 6). SOD1 is the primary enzyme, converting superoxide into H_2O_2 in the cytosol. Therefore, our findings were initially surprising because H_2O_2 was expected to decrease, not increase, upon SOD1 inhibition. However, our signaling pathway analysis identified that ATN-224, and the resulting increase in superoxide, inhibited GPX enzyme activities, leading to an increase in H_2O_2 and a subsequent hyperoxidation of PRXs that caused their inactivation. GPXs and PRXs are part of antioxidant enzyme systems that, together with GSH and NADPH, remove H_2O_2 from the cell and therefore buffer high H_2O_2 levels to keep them below the cytotoxic limit. Fridovich showed that superoxide radicals can inactivate GPXs (26), supporting our findings that ATN-224 inhibits the scavenging ability of H_2O_2 in NSCLC cells, which results in an increase in intracellular H_2O_2, subsequent cell death, and synergy with the GSH scavenger BSO.

We specifically identified H_2O_2-induced P38 MAPK as the target of ATN-224–mediated peroxide stress and cancer cell death (Supplemental Figure 6). These results are consistent with the observation that loss of P38α MAPK accelerates tumorigenicity in an oncogenic *Kras*–induced mouse model of lung cancer (32). Previous studies also indicated that JNK and P38 MAPKs phosphorylate and destabilize MCL1, leading to cell death upon oxidative stress (33). Indeed, we found that ATN-224–mediated SOD1 inhibition and the resulting increase in H_2O_2 led to a P38 MAPK–dependent decline in MCL1 protein expression and subsequent cell death (Supplemental Figure 6). MCL1 is highly expressed in various cancers, including NSCLCs, and overexpression of MCL1 contributes to the resistance against cancer therapeutics like BCL2/BCLXL inhibitors (31). We therefore predicted that ATN-224 would show a synergistic response with other antiapoptotic inhibitors because the combination of the drugs could circumvent

the compensation of the independent antiapoptotic BCL2 family members. In fact, we observed augmented cancer cell death in cells treated with ATN-224 and the BCL2/BCLXL inhibitor ABT-263, raising the possibility that the combination of ATN-224 and BCL2 inhibitors is efficacious against NSCLCs, including those harboring *KRAS* or *KRAS/TP53* mutations, and also against cancers resistant to therapeutics due to MCL1 overexpression. Combination therapy would also allow a further reduction of ATN-224 treatment doses in order to prevent possible cytotoxic side effects. In human phase 1 clinical trials, ATN-224 given daily at 330 mg/kg or 300 mg/kg resulted in hematologic adverse effects including anemia and neutropenia. Doses of less than 200 mg/kg/day of ATN-224 were well tolerated in patients and did not significantly affect blood cells (39). It is possible that the hematologic adverse effects at high doses of ATN-224 were due to MCL1 downregulation, because MCL1 has been shown to be required for the survival of hematopoietic stem cells (40). Thus, it would be of interest to investigate whether the combination of low doses of ATN-224 with BCL2/BCLXL inhibitors are efficacious in reducing NSCLC.

In summary, we have identified the SOD1 inhibitor ATN-224 as a potential targeted therapy for NSCLCs including those harboring *KRAS* and *KRAS/TP53* mutations, which are often predictors of poor prognosis. Our study holds promise for the design of future pro-oxidant therapies by identifying the importance of impairing the redox adaptation mechanisms of cancer cells. Based on our findings, we suggest the design of dual pro-oxidant therapies through the combination of ROS-generating agents with ROS-scavenging inhibitors (like ATN-224) in order to diminish the ability of cancer cells to adapt to either agent. Whether SOD1 inhibitors like ATN-224 synergize with other proapoptotic (ABT-263), pro-oxidant, and chemotherapeutic agents in vivo to reduce tumorigenicity or even angiogenesis and metastasis remains an interesting question for future therapeutic studies. Considering the large percentage of tumors harboring ROS-inducing oncogenic mutations (e.g., *KRAS*, *TP53*, *EGFR*), the testing of pro-oxidants like ATN-224 in various cancers either as single agents or in combination therapies should be considered.

Methods

Drugs and reagents. Choline tetrathiomolybdate (ATN-224) was a gift from Andrew Mazar (Northwestern University, Evanston, Illinois, USA). MnTBAP was purchased from A.G. Scientific. The kinase inhibitors SB203580 (P38), SP600125 (JNK), and FR180204 (ERK1/2) were purchased from Calbiochem. The antioxidants ebselen and NAC were purchased from Cayman Chemical and Sigma-Aldrich, respectively. The caspase inhibitor zVAD(OMe)-FMK was purchased from Enzo Life Sciences. ABT-263 was purchased from Selleck Chemicals. BSO, the P53 inhibitor pifithrin-α, xanthine, and xanthine oxidase were purchased from Sigma-Aldrich. All drugs and reagents were used at the concentrations indicated in the text.

Cell culture. Cells were incubated at 37°C and maintained at 5% CO_2. A549 cells were obtained from ATCC. The mouse adenocarcinoma cell line from tumors carrying a Cre-inducible $Kras^{G12D}$ allele and a conditional loss-of-function *Tp53* allele was a gift from Tyler Jacks (MIT, Cambridge, Massachusetts, USA). A549 and KP cells were grown in DMEM plus 10% FBS (GemCell), 5% penicillin and streptomycin (Cellgro), 5% L-glutamine (Invitrogen), and 5% HEPES buffer (Cellgro). NBECs were purchased from Lonza. Cells were cultured in bronchial epithelial cell growth medium that allows for differentiation (no retinoic acid) supplemented with bovine pituitary extract, hydrocortisone, human EGF, epinephrine, insulin, transferrin, triiodothyronine, and gentamicin/amphotericin-B. $Bax^{-/-}Bak^{-/-}$ and $Casp9^{-/-}$ MEFs and their wild-type controls were generated as previously described and were simian virus 40 transformed (41). The MEFs were gifts from Craig Thompson (Cancer Biology and Genetics Program, Memorial Sloan-Kettering Cancer Center, New York, New York, USA) and Richard Flavell (Yale University, New Haven, Connecticut, USA), respectively. $Bim^{-/-}$ $Puma^{-/-}$ MEFs and their wild-type controls were transformed with dominant-negative P53 and were gifts from Andreas Villunger (Innsbruck Medical University, Innsbruck, Austria). All MEFs were cultured as previously reported (41). Additional *KRAS*-mutant NSCLC cells, as well as wild-type *KRAS* NSCLC cells, $Bim^{-/-}$, $Puma^{-/-}$, and $Noxa^{-/-}$ MEFs are described in the Supplemental Methods.

shRNA knockdown experiments. The pLKO.1 vector (MISSION; Sigma-Aldrich) was used to express shRNAs targeting human SOD1. The following two hairpin sequences were used: 5′ CCGGGCTGTAGAAATGTATCCTGATCTCGAGATCAG GATACATTTCTACAGCTTTTTG 3′ (clone 8) and 5′ CCGGAGCAGATGACTTGGGCAAAGGCTCGA GCCTTTGCCCAAGTCATCTGCTTTTTTG 3′ (clone 44). The nonsilencing (scrambled control) shRNA was purchased from Addgene (plasmid 1864): 5′ CCTAAGGTTAAGTCGCCCTCGCTCTAGCGAGGGCGAC TTAACCTTAGG 3′. For lentiviral infection, the constructs were transfected along with packaging plasmids into HEK293T cells using Lipofectamine 2000 (Invitrogen). Viral supplements were collected 48 hours after transfection, and target cells were transiently infected in the presence of 8 μg/ml polybrene (Sigma-Aldrich). Cells were treated 48 hours after viral infection.

Retroviral and adenoviral gene expression. Human BCLXL was cloned into pBABE-puromycin vector (Addgene) using NotI and SwaI. Empty pBABE vectors were used as controls. The pLNCX vector containing human MCL1 was a gift from Aly Karsan (University of British Columbia, Vancouver, British Columbia, Canada). Briefly, for retroviral infections, constructs were transfected along with packaging plasmids into HEK293T cells using Lipofectamine 2000. Viral supplements were collected 48 hours after transfection, and target cells were infected in the presence of 8 μg/ml polybrene (Sigma-Aldrich). Cells were selected with puromycin (pBABE-puro) and G418 (pLNCX-MCL1). Cells were also infected with 5 and 10 PFUs per cell of adenoviruses encoding GPX1, SOD1, or an empty control adenovirus (ViraQuest). GPX1 and SOD1 adenoviral vectors were provided by John Engelhardt's laboratory (University of Iowa Vector Core, Iowa City, Iowa, USA). Cells were treated 24 hours after viral infection.

Western blots. Cells were lysed in cell lysis buffer (Cell Signaling Technology) supplemented with PMSF, and lysates were resolved on 7.5% to 12% Criterion gels (Bio-Rad) and transferred to nitrocellulose. The antibodies used were: SOD1 (4266), GPX1 (3206), CC3 (ASP175) (9664), PRX1 (D5G12) (8499), phospho-P38 MAPK (Thr180/Tyr182) (9211), P38 MAPK (9212), phospho-MAPKAPK2 (Thr222) (3316), MAPKAPK2 (3042), phospho-SAPK/JNK (Thr183/Tyr185) (9251), SAPK/JNK (9252), phospho-P44/P42 MAPK (ERK1/2) (Thr202/Tyr204) (4377), and P44/P42 MAPK (ERK1/2) (9102) (all from Cell Signaling Technology). PRX-SO_3 was purchased from Abcam. BCLXL (sc-8392) and MCL1 (sc-819) recognizing human proteins were purchased from Santa Cruz Biotechnology Inc. MCL1 recognizing mouse proteins was purchased from Rockland. The loading control antibodies actin and α-tubulin were purchased from Sigma-Aldrich.

Cell death assay. Cells were plated (4×10^4 cells/well) in 6-well tissue culture dishes and treated with the reagents indicated in the text for 96 hours. For human NSCLC cells, cell death was assessed using propidium iodine (PI) (Invitrogen). PI is a cell-impermeable intercalating agent that binds to nucleic acids, therefore, PI staining is excluded from live cells. The loss of membrane integrity in dead cells allows for PI uptake. Upon DNA binding, PI fluorescence is enhanced; the fluorescence excitation maximum is shifted 30–40 nm to the red, and the fluorescence emission maximum is shifted 15 nm to the blue. Cells were trypsinized and resuspended in PBS

containing 100 ng/ml PI. PI-positive cells were analyzed using flow cytometry (BD LSRFortessa; BD Biosciences). For KP cells, cell death was measured using trypan blue dye exclusion staining. Trypan blue is a diazo dye that can only traverse the cell membranes of dead cells. Dead cells acquire a distinctive blue color that is visible under a bright-field microscope. For trypan blue death assays, trypan blue–positive (dead) cells were counted in an automated method using the Vi-CELL XR Viability Analyzer (Beckman Coulter), which averages 50 counted images per sample.

Anchorage-independent soft agar assays. Cells were plated (500 cells/well) in 96-well tissue culture dishes. A two-layer agar system was used (Millipore), with 0.8% agarose in the bottom layer and 0.4% in the top layer, which contains the cells. Cells were drug treated 24 hours after seeding, then treated every 48 hours with fresh media and drugs, and stained after 21 days according to the manufacturer's protocol. Images of wells were taken with an inverted microscope at ×8 magnification (MZFLIII; Leica). The number of colonies over 100 μm were counted using ImageJ software (NIH).

SOD1 activity assay. Cells (3×10^5) were plated in 10-cm tissue culture dishes. Cells were lysed in cold buffer (20 mM HEPES, 1 mM EGTA, 210 mM mannitol, and 70 mM sucrose) 24 hours after drug treatment and homogenized. Lysates were centrifuged at 10,000 *g* for 15 minutes to separate cytosolic SOD1 from mitochondrial SOD2. Supernatant was used for SOD1 enzyme analysis. An enzyme assay was performed according to the manufacturer's protocol (706002; Cayman Chemical). Briefly, SOD1 activity was assayed by measuring the inhibition of reduction of the water-soluble tetrazolium salt [2-(4-iodophenyl)-3-(4-nitrophenyl)-5-(2,4-disulfo-phenyl)-2H-tetrazolium, monosodium salt], which produces a water-soluble formazan dye on reduction with a superoxide anion generated by xanthine oxidase.

ROS measurements. For H_2O_2 measurements, three techniques were used: (a) cells were incubated in 5 μM 5,6-chloromethyl-2′,7′-dichlorodihydrofluorescein diacetate, acetyl ester (CM-H_2DCFDA; Invitrogen) for 1 hour; (b) an adenoviral roGFP probe (ViraQuest) was used as previously described (3). Briefly, cells were infected with 50 PFU adenoviral roGFP, and the probe was calibrated by treating cells with 1 mM DTT for complete reduction and with 1 mM t-butyl H_2O_2 for complete oxidation. The percentage of oxidized probe was determined by using the formula: percentage of oxidized probe = X-DTT / H_2O_2-DTT; and (c) the H_2O_2 sensor roGFP2-thiol peroxidase (roGFP2-ORP1) was a gift of Tobias Dick (Cancer Research Center, Heidelberg, Germany). Cells were transiently infected with a retrovirus expressing roGFP2-ORP1, and cells were treated 24 hours postinfection. The probe was calibrated as described above. MFI for the three probes was measured by flow cytometry. The superoxide measurements are described in the Supplemental Methods.

GPX assay. Cells (3×10^5) were plated in 10-cm tissue culture dishes. Cells were lysed in cold buffer (50 mM Tris-HCL, 5 mM EDTA) 48 hours after drug treatment and homogenized. An enzyme assay was performed according to the manufacturer's protocol (703102; Cayman Chemical). Briefly, GPX activity was indirectly measured through a coupled reaction with glutathione reductase (GR). Oxidized glutathione, produced upon reduction of H_2O_2 to H_2O by GPX, is recycled back to its reduced state by GR and NAPDH. The oxidation of NADPH to $NADP^+$ was coupled to a decrease in absorbance at 340 nm (A_{340}). The rate of decrease in A_{340} is proportional to GPX activity.

Mouse therapeutic trial. *Lox-Stop-Lox Kras*$^{G12D/+}$ mice (22) and *Tp53*$^{fl/fl}$ mice were obtained from the National Cancer Institute Repository. Mice were inbred on a C57BL/6 background and crossed to generate *Lox-Stop-Lox Kras*$^{G12D/+}$ *Tp53*$^{fl/fl}$ mice. Lung tumors were induced by intratracheal inhalation of 10^7 PFUs of adenoviral Cre recombinase (ViraQuest), as previously described (42). Freshly prepared ATN-224 or PBS (control) (4 mg/kg) was administered by i.p. injection 8 weeks postinfection. Mice were treated every other day for 4 weeks. Three independent cohorts of mice were used, with 5 to 6 animals per cohort per condition. Mice were randomized to receive either drug or placebo treatments.

Lung tumor load and lesion number. Twelve weeks after adeno-Cre infection (4 weeks after the start of injections), mice were sacrificed and lungs were isolated and fixed in 4% formalin. Lung lobes were embedded in paraffin, step sectioned (500 μm), and stained with H&E. Stained lung sections were imaged at ×10 magnification using a Zeiss Axio Microscope, and all images were arranged using TissueFAXs (TissueGnostics) software to obtain a high-resolution image of each whole lung. Tumor area and total lung area were quantified using HistoQuest (TissueGnostics) software. Tumor burden was defined as the tumor-positive area divided by the total lung area. Lesion number was defined as the number of tumors per lung. Imaging and image analysis were performed at the Northwestern University Cell Imaging Facility (Chicago, Illinois, USA).

KI67 proliferation analysis and CC3 cell death analysis in lungs. Mouse lungs were sectioned as described in the previous section and stained for hematoxylin (nuclear stain) and either KI67 (Histo Scientific Research Laboratory) or CC3 (Mouse Histology and Phenotyping Laboratory, Northwestern University). Lung sections were analyzed at ×20 magnification using a Zeiss Axio Microscope. Images were arranged using TissueFAXs (TissueGnostics) software. The percentage of KI67- or CC3-positive cells in each lung was quantified using HistoQuest software. The number of KI67- or CC3-positive cells was divided by the total number of cells in each lung (hematoxylin counterstain).

Mitochondrial oxygen consumption rate measurement. The mitochondrial oxygen consumption rate measurement is described in the Supplemental Methods.

Statistics. GraphPad software was used for statistical analysis. Data are represented as the means ± SEM. Data were analyzed by using unpaired, 2-tailed Student's *t* tests when comparing two variables. A 2-tailed Mann-Whitney *U* test was used for the analysis of CC3-stained lung sections. *P* values less than 0.05 were considered significant.

Study approval. The IACUC of Northwestern University approved all animal studies and procedures.

Acknowledgments

We thank Tyler Jacks and Thales Papagiannakopoulos (MIT, Cambridge, Massachusetts, USA) for their expertise regarding the KP mouse model. We thank Ralph DeBerardinis (UT Southwestern, Dallas, Texas, USA) for his helpful comments on the manuscript. We also thank the Histo-Scientific Research Laboratories and the Mouse Histology and Phenotyping Laboratory for the histological preparations of lung sections. This work was supported by the LUNGevity Foundation and the Consortium of Independent Lung Health Organizations convened by the Respiratory Health Association of Metropolitan Chicago (to N.S. Chandel); by NIH grant R01CA123067 (to N.S. Chandel); F30ES019815 (to L.A. Sena); T32-HL76139 (to L.A. Sena); a Dixon Translational Grant (to N.S. Chandel); and a Northwestern University Malkin Scholar Award (to A. Glasauer). The Northwestern University Cell Imaging Facility is supported by CCSG P30 CA060553, awarded to the Robert H. Lurie Comprehensive Cancer Center. The content is solely the responsibility of the authors and does not necessarily represent the official views of the NIH.

Received for publication June 21, 2013, and accepted in revised form September 26, 2013.

Address correspondence to: Navdeep S. Chandel, 240 East Huron, McGaw Pavilion, M-334, Chicago, Illinois 60611, USA. Phone: 312.503.2549; Fax: 312.503.0411; E-mail: nav@northwestern.edu.

1. Herbst RS, Heymach JV, Lippman SM. Lung cancer. *N Engl J Med*. 2008;359(13):1367–1380.
2. Shaw AT, et al. Selective killing of K-ras mutant cancer cells by small molecule inducers of oxidative stress. *Proc Natl Acad Sci U S A*. 2011;108(21):8773–8778.
3. Weinberg F, et al. Mitochondrial metabolism and ROS generation are essential for Kras-mediated tumorigenicity. *Proc Natl Acad Sci U S A*. 2010; 107(19):8788–8793.
4. Wallace DC. Mitochondria and cancer. *Nat Rev Cancer*. 2012;12(10):685–698.
5. Cairns RA, Harris IS, Mak TW. Regulation of cancer cell metabolism. *Nat Rev Cancer*. 2011;11(2):85–95.
6. Ichijo H, et al. Induction of apoptosis by ASK1, a mammalian MAPKKK that activates SAPK/JNK and p38 signaling pathways. *Science*. 1997; 275(5296):90–94.
7. Hayes JD, McMahon M. NRF2 and KEAP1 mutations: permanent activation of an adaptive response in cancer. *Trends Biochem Sci*. 2009;34(4):176–188.
8. Schafer ZT, et al. Antioxidant and oncogene rescue of metabolic defects caused by loss of matrix attachment. *Nature*. 2009;461(7260):109–113.
9. Mitsuishi Y, et al. Nrf2 redirects glucose and glutamine into anabolic pathways in metabolic reprogramming. *Cancer Cell*. 2012;22(1):66–79.
10. Young TW, Mei FC, Yang G, Thompson-Lanza JA, Liu J, Cheng X. Activation of antioxidant pathways in ras-mediated oncogenic transformation of human surface ovarian epithelial cells revealed by functional proteomics and mass spectrometry. *Cancer Res*. 2004;64(13):4577–4584.
11. DeNicola GM, et al. Oncogene-induced Nrf2 transcription promotes ROS detoxification and tumorigenesis. *Nature*. 2011;475(7354):106–109.
12. Ren D, et al. Brusatol enhances the efficacy of chemotherapy by inhibiting the Nrf2-mediated defense mechanism. *Proc Natl Acad Sci U S A*. 2011; 108(4):1433–1438.
13. Raj L, et al. Selective killing of cancer cells by a small molecule targeting the stress response to ROS. *Nature*. 2011;475(7355):231–234.
14. Trachootham D, et al. Selective killing of oncogenically transformed cells through a ROS-mediated mechanism by β-phenylethyl isothiocyanate. *Cancer Cell*. 2006;10(3):241–252.
15. Somwar R, et al. Superoxide dismutase 1 (SOD1) is a target for a small molecule identified in a screen for inhibitors of the growth of lung adenocarcinoma cell lines. *Proc Natl Acad Sci U S A*. 2011; 108(39):16375–16380.
16. Donate F, et al. Identification of biomarkers for the antiangiogenic and antitumour activity of the superoxide dismutase 1 (SOD1) inhibitor tetrathiomolybdate (ATN-224). *Br J Cancer*. 2008; 98(4):776–783.
17. Juarez JC, et al. Superoxide dismutase 1 (SOD1) is essential for H2O2-mediated oxidation and inactivation of phosphatases in growth factor signaling. *Proc Natl Acad Sci U S A*. 2008;105(20):7147–7152.
18. Lee K, et al. The copper chelator ATN-224 induces peroxynitrite-dependent cell death in hematological malignancies. *Free Radic Biol Med*. 2013;60:157–167.
19. Antonarakis ES, Zahurak ML, Lin J, Keizman D, Carducci MA, Eisenberger MA. Changes in PSA kinetics predict metastasis-free survival in men with PSA-recurrent prostate cancer treated with nonhormonal agents: combined analysis of 4 phase II trials. *Cancer*. 2012;118(6):1533–1542.
20. Lin J, et al. A non-comparative randomized phase II study of 2 doses of ATN-224, a copper/zinc superoxide dismutase inhibitor, in patients with biochemically recurrent hormone-naive prostate cancer. *Urol Oncol*. 2013;31(5):581–588.
21. Singh M, et al. Assessing therapeutic responses in Kras mutant cancers using genetically engineered mouse models. *Nat Biotechnol*. 2010;28(6):585–593.
22. Jackson EL, et al. Analysis of lung tumor initiation and progression using conditional expression of oncogenic K-ras. *Genes Dev*. 2001;15(24):3243–3248.
23. Juarez JC, et al. Copper binding by tetrathiomolybdate attenuates angiogenesis and tumor cell proliferation through the inhibition of superoxide dismutase 1. *Clin Cancer Res*. 2006;12(16):4974–4982.
24. Meyer AJ, Dick TP. Fluorescent protein-based redox probes. *Antioxid Redox Signal*. 2010;13(5):621–650.
25. Winterbourn CC, Hampton MB. Thiol chemistry and specificity in redox signaling. *Free Radic Biol Med*. 2008;45(5):549–561.
26. Blum J, Fridovich I. Inactivation of glutathione peroxidase by superoxide radical. *Arch Biochem Biophys*. 1985;240(2):500–508.
27. Tait SW, Green DR. Mitochondria and cell death: outer membrane permeabilization and beyond. *Nat Rev Mol Cell Biol*. 2010;11(9):621–632.
28. Beroukhim R, et al. The landscape of somatic copy-number alteration across human cancers. *Nature*. 2010;463(7283):899–905.
29. Weir BA, et al. Characterizing the cancer genome in lung adenocarcinoma. *Nature*. 2007; 450(7171):893–898.
30. Wei G, et al. Chemical genomics identifies small-molecule MCL1 repressors and BCL-xL as a predictor of MCL1 dependency. *Cancer Cell*. 2012; 21(4):547–562.
31. Chen S, Dai Y, Harada H, Dent P, Grant S. Mcl-1 down-regulation potentiates ABT-737 lethality by cooperatively inducing Bak activation and Bax translocation. *Cancer Res*. 2007;67(2):782–791.
32. Dolado I, Swat A, Ajenjo N, De Vita G, Cuadrado A, Nebreda AR. p38α MAP kinase as a sensor of reactive oxygen species in tumorigenesis. *Cancer Cell*. 2007;11(2):191–205.
33. Inoshita S, et al. Phosphorylation and inactivation of myeloid cell leukemia 1 by JNK in response to oxidative stress. *J Biol Chem*. 2002;277(46):43730–43734.
34. Tse C, et al. ABT-263: a potent and orally bioavailable Bcl-2 family inhibitor. *Cancer Res*. 2008; 68(9):3421–3428.
35. Griffith OW, Meister A. Potent and specific inhibition of glutathione synthesis by buthionine sulfoximine (S-n-butyl homocysteine sulfoximine). *J Biol Chem*. 1979;254(16):7558–7560.
36. Fath MA, Ahmad IM, Smith CJ, Spence J, Spitz DR. Enhancement of carboplatin-mediated lung cancer cell killing by simultaneous disruption of glutathione and thioredoxin metabolism. *Clin Cancer Res*. 2011;17(19):6206–6217.
37. Sordella R, Bell DW, Haber DA, Settleman J. Gefitinib-sensitizing EGFR mutations in lung cancer activate anti-apoptotic pathways. *Science*. 2004;305(5687):1163–1167.
38. Berenson JR, et al. Phase I study of the [Cu, Zn] superoxide dismutase (SOD1) inhibitor ATN-224 (Bis-choline tetrathiomolybdate) in patients (pts) with advanced hematologic malignancies. *Blood*. 2006;108(11):2593.
39. Lowndes SA, et al. Phase I study of copper-binding agent ATN-224 in patients with advanced solid tumors. *Clin Cancer Res*. 2008;14(22):7526–7534.
40. Opferman JT, et al. Obligate role of anti-apoptotic MCL-1 in the survival of hematopoietic stem cells. *Science*. 2005;307(5712):1101–1104.
41. Snyder CM, Shroff EH, Liu J, Chandel NS. Nitric oxide induces cell death by regulating anti-apoptotic BCL-2 family members. *PLoS One*. 2009;4(9):e7059.
42. DuPage M, Dooley AL, Jacks T. Conditional mouse lung cancer models using adenoviral or lentiviral delivery of Cre recombinase. *Nat Protoc*. 2009; 4(7):1064–1072.